Toward the development of sensors for lung cancer: the adsorption of 1-propanol on hydrophobic zeolites

K. Boukair, J. Marcos Salazar, Guy Weber, M. Badawi, S. Ouaskit, J.-M. Simon

Toward the development of sensors for lung cancer: the adsorption of 1-propanol on hydrophobic zeolites

K. Boukair,[1] J. M. Salazar,[2] G. Weber,[2] M. Badawi,[3] S. Ouaskit,[1] and J.-M. Simon[2]
[1)] *Laboratoire de Physique de la Matière Condensée, Hassan 2 University, Casablanca, Morroco.*
[2)] *ICB-UMR 6303 CNRS, Bourgogne Franche Comté University, Dijon, France.*
[3)] *Laboratoire de Physique et Chimie Thoriques, University of Lorraine, Nancy, France.*

(*Electronic mail: jmsimon@u-bourgogne.fr)

(Dated: 4 October 2023)

A healthy breath is mainly composed of water, carbon dioxide, molecular nitrogen and oxygen and it contains many species, in small quantities, which are related to the ambient atmosphere and the metabolism. The breath of a person affected by lung cancer presents a higher concentration of 1-propanol than usual. In this context, the development of specific sensors to detect 1-propanol from breath is of high interest. The amount of propanol usually detected in the breath is of few ppb, this small quantity is a handicap for reliable diagnostic. This can be overcome if the sensor is equipped with a pre-concentrator. Our studies search to provide an efficient material playing this role. This will contribute to the development of easy to use reliable lung cancer detectors. For this we investigate the properties of some hydrophobic porous materials (chabazite, silicalite-1 and dealuminated faujasite). The use of hydrophobic structures is to avoid the saturation of the material with the water of the exhaled breath. Our experimental and simulation results suggest that the silicalite -1 (MFI) is the most suitable structure.

I. INTRODUCTION

Volatile organic compounds (VOC's) are natural toxic pollutants resulting from combustion, oil evaporation, paintings and other human activities. The VOC's are small molecules of various chemical types (e.g., small aldehydes, alcohol, benzoic compounds, etc.). They are characterized by a high volatility and they spread with ease in the atmosphere. Furthermore, once in the air, they can react with other gases to generate other airborne pollutants.

The exhaled breath contains over 2000 components including VOC's (e.g., ethanol, xylene, propanal, propanol, etc.), non-volatile organic compounds (e.g., proteins, sugars) and volatile inorganic compounds (e.g., CO_2, N_2, H_2O). The concentration variation and/or the presence of certain VOC's, like 1-propanol, in the breath of a patient might indicate a gastric cancer[1–3], a breast cancer[4,5] or a lung cancer[6–10]. The 1-propanol[11–14] is metabolized and exhaled. Its presence in the breath above a threshold concentration (5.6-473.3 ppb[13], 236.2 ppb[15], 4.37-13.15 ppb[16]) suggests a patient suffering of lung cancer.

This type of cancer is difficult to diagnostic in its early stage and is considered as one of the most serious public health problem of the century given its high mortality rate[17,18]. Henceforth, researchers are challenged for developing new non-invasive technologies, exploiting the biomarkers present in the breath exhalation in less than an hour. A promising approach is to use gas sensors for trapping 1-propanol. These sensors are equipped with a pre-concentrator containing a porous material: zeolites[19–21]. A non negligeable number of zeolites (over 250 distinct types of zeolite[22,23]) can be used. They are known for their high surface area, their thermal stability, their selectivity for adsorbing different types of VOC's[24–28]. In many industrial applications zeolites are used for analyzing airborne gases on sensors[29].

Human breath contains a high proportion of water and carbon dioxide in comparison with VOC's. Hence, the best zeolites for adsorbing 1-propanol has to be hydrophobic to prevent a competitive adsorption with water[19,30–33]. The most frequent zeolites used for sieving VOC's in the presence of water are: chabazite (CHA), silicalite-1 (MFI), de-aluminated Y faujasite (DAY), beta zeolite, natural stilbite and LTA[34–38].

Studies on the adsorption of alcohols by zeolites give the structure that adsorbs the most[30,35,39–41]. M. Sakuth *et al.*,[42] illustrated how the surface polarity affects the adsorption of a polar and non-polar component such as 1-propanol and toluene. The adsorption of formaldehyde on the zeolite of type faujasite in the presence of water has been studied by Bellat *et al.*,[26] their results show an increase of adsorption for formaldehyde by using DAY. The work of Gregis *et al.*,[19] is focussed on the development of a small breath analyzer of toluene, propanol, o-xylene, cyclohexane.

Our work consist on studying the adsorption of 1-propanol, carbon dioxide, molecular nitrogen and water on three different hydrophobic siliceous zeolites: CHA, MFI , and DAY. For these, we developed Monte-Carlo simulations in the grand canonical ensemble (GCMC). The studies are performed at 20, 35 and 50°C. Simulated data obtained at 25°C are compared with experimental results for the adsorption of water and 1-propanol on the three investigated zeolites. The adsorption isotherms, thermodynamic (isosteric heat of adsorption) and structural quantities (pair distribution function) are computed for developing a physical insight about the interactions

between the adsorbent and adsorbate and determine the most suitable zeolite to be used as a preconcentrator.
The paper is organised as follows: In Section II we provide details of the GCMC simulations and experiments. Next, we discuss the results in section III. Finally, the main conclusions of our studies are summarised in the last section.

II. EXPERIMENTAL AND SIMULATIONS DETAILS

A. Experimental details

1. Adsorbents

Experimentally we studied two types of zeolites: a pure hydrophobic zeolite DAY, supplied by Degussa, and a purely siliceous MFI zeolite (synthesized in fluoride medium by the Mulhouse Materials Science Institute). The chemical formula of DAY is $Na_2(Al_2Si_{190}O_{384})$, that for MFI is $Si_{96}O_{192}$. In table I are listed the porous characteristics of the adsorbents, which were characterized by nitrogen adsorption-desorption at 77 K.

TABLE I: Some physical properties of DAY and silicalite-1 (S_{BET}: specific surface area; V_μ: micropore volume determined by the t-method; V_{meso}: mesoporous volume approximated from the difference between V_T and V_μ), where V_T is the total pore volume at a pressure, $P \approx 0.97P_0$ with $P_0 = 1$atm.

Adsorbent	Si/Al ratio	3D Porous system	S_{BET} (m^2/g)	V_μ (cm^3/g)	V_{meso} (cm^3/g)
DAY	95	two interconnected sets of α-cages and and β-cages with a free aperture diameter of around 7.4 Å and 2.2 Å, respectively	717	0.293	0.087
Silicalite-1	> 500	Two distinct straight and sinusoidal channels of size $5.3 * 5.6$ Å^2 along [010] and $5.5 * 5.1$ Å^2 along [100], respectively	750	0.190	-

2. Adsorbates

Distilled water and 1-propanol distributed by Merck (purity higher than 99.5%) are employed for adsorption measurements. Prior to use, 1-propanol is transferred to a flask containing an activated zeolite 3A in order to trap residual water.

3. Measurements of the adsorption-desorption isotherms for 1-propanol and water

1-Propanol and water adsorption-desorption isotherms are measured using a home-made McBain thermobalance, equipped with a quartz spring using the ultra-high vacuum technology. The gas pressure, inside the balance, is measured with Baratron sensors.
For eliminating the gases adsorbed at room temperature, in particular water, 10 to 15 mg of zeolite samples are first degazed under a dynamic vacuum of 10^{-5} hPa for 5h at 400°C. Afterwards, the sample is cooled down to 25°C. The adsorption branch of the isotherm is obtained step by step by using a static method: introduce progressively doses of 1-propanol or water vapor into the thermobalance. Once an equilibrium state (i.e., constant mass) is reached the mass value is recorded. Subsequently, the pressure is slightly increased for obtaining a new equilibrium state. This procedure is applied up to saturation. For the desorption branch, the pressure is decreased progressively from saturation, in an analogous way as for the adsorption, down to vacuum (see Refs[43–48] for more details). The pressure range investigated starts at 10^{-4} hPa up to the saturation pressure (28.00 or 31.64 hPa for 1-propanol and water, respectively). The accuracies of temperature, pressure and weight measurements are ±1°C, ± 0.001 hPa and ± 0.01 mg, respectively.

B. Models and simulations details

Adsorption of H_2O, C_3H_8O, CO_2 and N_2 has been investigated by GCMC simulations in the (μ, V, T)-ensemble. The simulations are performed with three different types of hydrophobic zeolites: CHA, MFI and DAY

(see Fig.1). The analyzed temperatures are 20, 25, 35 and 50°C for distinguishing the impact of the temperature on the affinity of adsorption. The imposed fugacity range between 10^{-2} Pa and 10^5 Pa. We used the GOMC software[49] for the simulations. This Monte-Carlo package has been optimized for simulating phase equilibria and physical properties of complex fluids.

For single gas adsorption, the insertion/deletion movements correspond to 50% of the grand total moves while the remaining correspond to 10% of rigid body displacement, 10% of rotation, 10% of crankshaft, 10% of regrowth and 10% of intraswap. The crankshaft movement is a method to improve the sampling of long chain molecules by turning a part of the molecule around a bond axis (simulating a rotation or a torsion action). We used a coupled, biased selection for the intermolecular energy and a decoupled, biased selection for the bending and torsional energies to make the crankshaft movement more effective. The intraswap movement is a technique to remove a molecule from a box and insert it back into the same box using coupled-decoupled configurational-bias algorithm. The regrowth movement is a technique to delete and regrow a part of the molecule using coupled-decoupled configurational-bias algorithm. The frameworks are considered as rigid. The crystallographic atomic positions of the zeolites are those given by the International Zeolite Association[22]. We applied 3D periodic boundary conditions to the crystal, see Table II. The simulations are equilibrated by using a minimum of 3×10^7 steps. The analyzed data follows after equilibration and includes 4×10^7 steps. The cutoff distance for the van der Waals interactions has been taken as half the smaller axis of the simulation box. For the Coulomb interactions we used the Ewald method with a precision of 1×10^{-6}.

The unit cell of the chabazite is composed of 36 Si atoms and 72 O atoms. The pore diameter of this structure is 7.37 Å. The DAY faujasite contains 192 Si atoms and 384 O atoms with an pore diameter of the supercages is 11.24 Å. For MFI the unit cell has 96 Si atoms and 192 O atoms, its pore diameter is 6.36 Å. The adsorbates and zeolites were modelled using the all-atom model excepting the methylene (CH_2) and methyl (CH_3) groups which are represented by one center of force localized on the carbon atom. The adsorbate molecules interact with the zeolites and other adsorbates through the Lennard-Jones (LJ) potential and the electrostatic interactions:

TABLE II: Structural properties of the simulated zeolites

zeolite type	cristaline form	S lattice parameter (in Å)	supercell
CHA	Hexagonal	13.675 * 13.675 * 14.767	3*3*3
DAY	Cubic	24.276 * 24.276 * 24.276	2*2*2
MFI	Orthorhombic	20.09 * 19.738 * 13.142	2*2*3

$$U_{ij} = 4\epsilon_{ij}\left[\left(\frac{\sigma_{ij}}{r_{ij}}\right)^{12} - \left(\frac{\sigma_{ij}}{r_{ij}}\right)^{6}\right] + \frac{q_i q_j}{4\pi\epsilon_0 r_{ij}}, \quad (1)$$

where ϵ_{ij} and σ_{ij} are the LJ potential well depth and diameter, respectively. r_{ij} is a distance between a pair of atoms i and j, q_i and q_j are the partial charges of atoms i and j and ϵ_0 is the vacuum permittivity.

The LJ interaction potential parameters and electric charges have been taken from the literature and given in Tables (III, IV, IX, X and XI) for the zeolites[50], 1-propanol[51], carbon dioxyde[52], nitrogen[53] and water. For the last one we used the TIP4P-2005[54] model and for the zeolites the force field TraPPE-zeo[50].

The electric charges are localized on the atoms. For N_2 a quadripole is modelled by adding a charge on the center of mass of the molecule. The LJ parameters between species of different types are obtained from the Lorentz-Berthelot mixing rules (Eq.2). For reproducing the experimental isotherm of 1-propanol at 25°C, for DAY and MFI, the depth of the LJ potential has been adjusted for the interaction between propanol and oxygen of the zeolite (Table V). Moreover, this adjustment has been also used for the adsorption of 1-propanol in the chabazite. The simulated adsorbates have been considered rigid, but 1-propanol which includes internal degrees of freedom (c.f. stretching, bending and torsion) (Tables VI, VII, VIII).

$$\sigma_{ij} = \frac{\sigma_i + \sigma_j}{2} \qquad \epsilon_{ij} = \sqrt{\epsilon_i \epsilon_j} \quad (2)$$

III. RESULTS AND DISCUSSION

A. Adsorption isotherms

The adsorption isotherms are given in Figures 2-5 for 1-propanol, water, carbon dioxyde and nitrogen. They are presented in terms of number of molecules per unit cell (molec./u.c.), N_{ads}, as a function of either fugacity f (for the simulation results) or pressure P (for experimental data). As expected, N_{ads} increases as the temperature decreases for a given fugacity and the isotherms are shifted towards lower fugacities as temperature decreases. Notice that for DAY the molecules are located in the α cages and none in the β cages in agreement with previous

TABLE III: Zeolite interaction potential parameters[50], O_z is the oxygen atom of the zeolite.

Atoms	ϵ/k_B (K)	σ(Å)	charge(e)
Si	22	2.3	1.5
O_z	53	3.3	-0.75

TABLE IV: 1-Propanol interaction potential parameters[51]. O_a and H_a are the oxygen and hydrogen atoms of the alcohol function. $CH2_{OH}$ is the function bonded to the OH group.

Atoms	ϵ/k_B (K)	σ(Å)	charge(e)
CH3	98	3.75	0.0
CH2	46	3.95	0.0
$CH2_{OH}$	46	3.95	0.265
O_a	93	3.02	-0.7
H_a	0.0	0.0	0.435

TABLE V: Modification LJ parameters for 1-propanol zeolite interaction.

Atoms	ϵ/k_B (K)	σ(Å)
CH_3 - O_z	74	3.525
O_a - O_z	95.04	3.16

H_a:$H_{Propanol}$, O_a:$O_{Propanol}$, O_z:$O_{Zeolite}$.

TABLE VI: Fixed bond lengths.

Stretch type	Length (Å)
CH_3-CH_2	1.54
CH_2-CH_2	1.54
CH_2-O_a	1.43
O_a-H_a	0.945

TABLE VII: Bending parameters.

$U_{bend}(\theta) = \frac{k_\theta}{2}(\theta - \theta_{eq})^2$

Bend type	$\theta(^\circ)$	k_θ/k_B (K/rad^2)
CH_3-CH_2-CH_2	114	62500
CH_2-CH_2-O_a	109.47	50400
CH_2-O_a-H_a	108.50	55400

θ the bending angle, k_θ is force constant.

studies. An overview of the influence of the presence or absence of cations on the adsorption of water molecules in zeolites with β cages is given in Refs[55–60] .

1. Adsorption of 1-propanol

For 1-propanol, the simulated isotherms at 25°C with the parameters of TraPPE-zeo[50] does not agree with our experiments (Figure 1 of Supplementary Material). Therefore, we adjusted the ϵ parameter of the Lennard-Jones potential for the interaction between the 1-propanol and the oxygen of the zeolite (Table V). This ensures a better compatibility between simulations and experiments. For the CHA the adsorption isotherms revealed a classical S-shape. For DAY and MFI the adsorption isotherm obtained seems to occur in two steps, first a steep increase below a threshold of 30 molec./u.c. and 8 molec./u.c., respectively and followed by a less steeper slope. These last indicates a different mechanism of adsorption between CHA and the two other zeolites. At 20°C, the adsorption starts at 1 Pa for MFI and CHA and at 10 Pa for DAY. The amount of 1-propanol increases up to 10^5 Pa where it tends to a saturated plateau: around 6 molec./u.c. for CHA, 55 molec./u.c. for DAY and 12 molec./u.c for MFI, independently of the temperature. For DAY and MFI the simulation results are confronted with those obtained experimentally at 25°C. It can be corroborated in Figs. 2.b and c where the isotherms at 25°C exhibit a good agreement with experiments. Worthwhile to mention that for DAY the experimental isotherm starts at 1 Pa. It is plausible that the presence of some cations may enhance the adsorption of alcohol groups.

2. Adsorption of water

The simulated isotherms show an abrupt adsorption starting near $\approx 2.10^3$ Pa at 20°C. For the other temperatures the intake is shifted to higher pressures. For all temperatures, the saturation thresholds are $\approx$ 35 molec./u.c, 250 molec./u.c and 40 molec./u.c for CHA, DAY, and MFI, respectively. At 25°C, the simulated adsorption of water starts at fugacities higher than $\approx$ 3000 Pa (Fig. 3). This pressure is higher than the condensation pressure of the TIP4P-2005 model (801.8 Pa[61]). Obviously, these results reflect the fact that the zeolites used are hydrophobic. For DAY and MFI, the simulated results are in good agreement with experimental data.

Some authors[55–60,62–68] highlighted the impact of local defects or cations in zeolites on water adsorption and has been shown that they affect the adsorption in general. Simulations and experiments show that the condensa-

TABLE VIII: Torsion parameters.

$U_{torsion}(\phi) = C_1[1 + cos(\phi)] + C_2[1 - cos(2\phi)] + C_3[1 + cos(3\phi)]$

Torsion type	C_1/k_B	C_2/k_B	C_3/k_B
CH_3-CH_2-CH_2-O_a	176.62	-53.34	769.93
CH_2-CH_2-O_a-H_a	209.82	-29.17	187.93

ϕ the torsional angle, $C_{i\in(1,2,3)}$ are force constants in K.

TABLE IX: Carbon dioxide interaction potential parameters[52]. Cc and Oc is the carbon and oxygen atom of the carbon dioxyde.

Atoms	ϵ/k_B (K)	σ(Å)	charge(e)
Cc	28.129	2.757	0.6512
Oc	80.507	3.033	-0.3256

TABLE X: Nitrogen interaction potential parameters[53]

Atoms	ϵ/k_B (K)	σ(Å)	charge(e)
N	36.4	3.32	-0.482
Center of mass	-	-	0.964

tion transition is shifted (to lower pressure) as the number of local defects increases. The adsorption starts at pressure/fugacity values slightly higher than the condensation pressure of bulk water. Our experimental adsorption isotherm of water on silicalite-1 with small fraction of defects and with a high Si/Al ratio is in agreement with our simulated results. Moreover, Krishna et al.[30], studied the adsorption of water using the TIP5PEw model and showed that CHA, FAU, MFI have a hydrophobic behavior as we observed in our experiments and simulations.

We obtained that 1-propanol is adsorbed at lower pressures, approximately two orders of magnitude, than water. This suggest that zeolites should be selective for 1-propanol. This effect is more pronounced for MFI and CHA than for DAY.

3. Adsorption of carbon dioxyde and nitrogen

The shape of CO_2 and N_2 isotherms are rather similar independently of the zeolite structure. The adsorption starts at 2 10^3 Pa, Fig.4 and 5. Worthwhile to remark that the adsorbed amount of CO_2 and N_2 is much lower than 1-propanol and water. This is not surprising since it is well-known that CO_2 and N_2 are poorly adsorbed at room temperature. It is expected that these molecules should not compete with water and 1-propanol. Our results are in good agreement with data published in Ref[69].

TABLE XI: Water interaction potential parameters[54] . Ow is the oxygen atom of the water molecule.

Atoms	ϵ/k_B (K)	σ(Å)	charge(e)
H	-	-	0.5564
Ow	93.2	3.1589	-
Center of mass	-	-	-1.1128

B. Isosteric heat of adsorption

For understanding the different behaviors of the adsorbates, we have calculated the isosteric heat of adsorption, Q_{st}, for each zeolite studied. Indeed, in GCMC simulations it is straightforward to calculate Q_{st} from the fluctuations of internal energy U and the fluctuations of the number N of adsorbate molecules:

$$Q_{st} = RT - \frac{\langle \delta U \delta N \rangle}{\langle \delta N \delta N \rangle}, \tag{3}$$

where R is the ideal gas constant, T the temperature, $\langle\rangle$ denotes an ensemble average in the grand canonical ensemble and $\delta X = X - \langle X \rangle$ for a variable X.

Fig. 6 gives Q_{st} as a function of N_{ads} for 1-propanol (a), water (b), carbon dioxyde (c), and nitrogen (d). In this figure, the values of Q_{st} are obtained at 35°C (the statistical uncertainty of each point is lower than 5%). These results are very close independently of the temperatures. Therefore, we only present the heat of adsorption at 35°C. As shown on Figs 6 the heat of adsorption increases with the number of molecules adsorbed on the porous structure. This effect is more pronounced for 1-propanol and water in CHA and DAY. This tendency is enhanced for DAY due to its bigger pores that can trap more molecules in close contact. Notice that for water the values of Q_{st} become higher than H^{Vap} for high loadings. This can explain the steep step isotherms: when a molecule of water is adsorbed it creates, by itself, an hydrophilic site in the porous structure where additional water molecules can be trapped. For N_2 and CO_2, the heat of adsorption remains almost constant.

Table XII provides the extrapolated values of Q_{st} at zero loading and the experimental heats of evaporation, H^{Vap}, are also given. If we compare the heat of evaporation of water with Q_{st} the later is significantly lower. Which corroborates the hydrophobic nature of pure silica

materials.

For the four adsorptives and for the three zeolites the calculated values of the heat of adsorption, at zero coverage, are in good agreement with previous data (Table XII). It is noticeable that the values of Q_{st} are higher for MFI and CHA than for DAY, excepting N_2. We see a difference of approximately 25 kJ/mol between MFI and DAY. This energy variation may arise due to the difference of pore diameters or accessible pore volumes. That is to say; smaller the diameter is, higher the local density of molecules inside implying an enhance of interaction energy. We recall the pore diameters for MFI (6.36 Å) and CHA (7.37 Å) and DAY (11.24 Å).

For illustrating the difference of heat adsorption for water and 1-propanol we give an histogram of Q_{st} on Fig. 7. Once again we remark that the energy difference is in favour of 1-propanol compare to water and the best results are obtained for MFI.

TABLE XII: Heats of adsorption at zero coverage and heat of evaporation of C_3H_8O, H_2O, CO_2 and N_2 on CHA, DAY and MFI at room temperature. The experimental data and simulated values taken from the literature are given in the exp. and sim. lines, the lines sim*. are our simulated results. The values are given in kJ/mol.

		C_3H_8O	H_2O	CO_2	N_2
CHA	exp.	..	..	22.5[70]	13.6[69]
	sim.	..	..	23.7[69]	12.5[69]
	sim*.	47.8	38.3	24.4	12.5
DAY	exp.	..	50[65]	17.9[71]	..
	sim.	..	..	17.5[71]	..
	sim*.	40.1	32.7	22.6	15.2
MFI	exp.	64.9[72]	38[73]	24.1[74]	16.2[69] , 15.1[74]
	sim.	54[75]	32.5[76] , 43[77]	24.6[69]	13.9[69]
	sim*.	64.4	41.2	27.2	15.5
	H^{Vap}	47.32[78]	44.0 ,45.56[54]	16.7	5.57

C. Radial Distribution Function

The Radial Distribution Function (RDF), $g(r)$, characterizes the probability of finding a particle at a given distance, r, from another particle. This function is used for studying the local structure of a system, such as the arrangement of atoms or molecules in a crystal framework or the dispersion of ions in a solution. The integration of $g(r)$ yields the average coordination number, CN:

$$CN = 4\pi \int_0^r \rho g(r) r^2 dr, \tag{4}$$

where ρ is the density.

1. RDF for water

For gaining a physical insight of the interactions between the host structures and adsorbates we developed a local structure analysis inside the zeolites. For this we computed the RDF's and CN (Eq.4) at 10^5Pa, see Figs 8, 9, 10.

For the O_{water}-H_{water} RDF the first peak appears near 0.95 Å and corresponds to the intramolecular OH distance. The second peak at 1.8 Å is characteristic of the hydrogen bonds between adjacent water molecules. The O_{water}-O_{water} RDF's with a first peak around 2.8 Å show the presence of close water molecules (as we suggested in the discussion of the isotherms, see Fig.3). The coordination number, CN of O_{water}-O_{water} is approximately of 4.5 for DAY and 3 for CHA and MFI. The bigger the size of the pore is, the higher is the probability for trapping water molecules in close contact. This value of 4.5 is close the coordination number of liquid water (CN=4.7) and suggest that there is enough space in the α cages allowing, a probable, arrangement of water molecules similar to a liquid.

The RDF of O_{zeo}-H_{water}, see Supplementary Material, reveals no peak at 1.8 Å. This last indicates that there are no hydrogen bonds between H_2O and the framework.

2. RDF for 1-propanol

In Figs 11-13 are given the $g(r)$ at different loadings of 1-propanol in CHA, DAY and MFI. The intramolecular $O_{propanol}$-$H_{propanol}$ peak appears near 1Å. For intermolecular distances, the first peak in the RDF's of $O_{propanol}$-$O_{propanol}$ and $O_{propanol}$-$H_{propanol}$ appears at 2.74 Å and 1.8 Å, respectively. This last peak indicates the presence of hydrogen bonds between the hydrogen and the oxygen of the alcohol groups. By integrating $g(r)$ up to the first peak, the coordination numbers of $O_{propanol}$ - $O_{propanol}$ increases with loading for reaching the values of 0.8, 1.2 and 0.9 at 10^5Pa for the CHA, DAY and MFI, respectively. These values indicate that the hydroxyl groups tend to attract each other to form dimers of alcohols inside the pores.

For water and 1-propanol, the tendency of OH for creating hydrogen bonds with other OH groups explains the large increase of the heat of adsorption when the number of molecules increases.

The RDF of O_{zeo}-$H_{propanol}$, in Supplementary Material, reveals no peak at 1.8 Å. Like for water this indicates that there are no hydrogen bonds between 1-propanol and the framework.

IV. CONCLUSION

We developed GCMC simulations for three well-known siliceous zeolites (CHA, DAY and MFI). The simulation

work was performed in a range of temperature between 20 and 50°C and for some of the chemicals present in the exhaled breath. These simulations were developed for calculating the isotherms of water, 1-propanol, N_2 and CO_2. Experimental isotherms of adsorption of 1-propanol and water in DAY and MFI were also measured at 25°C and presented in this study.

Our work is fully oriented to provide the most efficient zeolite structure that can be used as a pre-concentrator of 1-propanol. This molecule is a biomarker indicating the presence of lung cancer. The zeolite we search for will be inside a ready to use cancer sensor, for analyzing the exhaled breath of patients. For this i) we calculated the isotherms of water, 1-propanol, N_2 and CO_2 on three hydrophobic siliceous zeolites. These isotherms show that the starting adsorption pressure of water is greater than for 1-propanol. This suggest that 1-propanol will be adsorbed in first place. In other words, water will not inhibit the adsorption of 1-propanol at low loading and low partial pressure. ii) The calculated isosteric heat of adsorption suggest that the best zeolite structure for adsorbing 1-propanol, in the range of temperature investigated, is the MFI. iii) We observe that hydrogen bonding does not govern the adsorption of 1-propanol molecules at low loading. This result is particularly interesting because it corresponds to the operational conditions of the sensors.

The perspectives of this work will be to study mixtures of exhaled breath compounds.

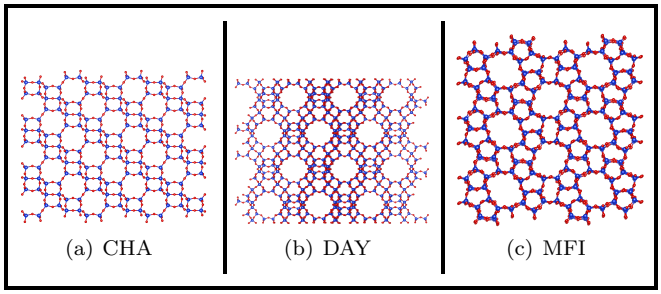

FIG. 1: Atomic representation of the zeolite structures of (a) CHA, (b) DAY and (c) MFI, in red the oxygen atoms and in blue the Si atoms.

SUPPLEMENTARY MATERIAL

The supplementary material presents a comparison of adsorption isotherms of 1-propanol obtained with TraPPEZeo potential using original and modified parameters with our experimental results. It also shows the radial distribution function of the oxygen atoms of the zeolites (CHA, DAY, MFI) with the hydrogen atoms of the adsorbed molecules of water and of the alcohol group of adsorbed 1-propanol.

Acknowledgments: We thank the CRI-CCUB Université de Bourgogne for giving us access to the computing facilities. We thank the EUR EIPHI, FEDER and the region Bourgogne-Franche Comté for financial support.

[1]K. Linderborg, T. Marvola, M. Marvola, M. Salaspuro, M. Farkkila, and S. Väkeväinen, "Reducing carcinogenic acetaldehyde exposure in the achlorhydric stomach with cysteine," Alcoholism: Clinical and Experimental Research **35**, 516–522 (2011).

[2]J. Zhang, Y. Tian, Z. Luo, C. Qian, W. Li, and Y. Duan, "Breath volatile organic compound analysis: An emerging method for gastric cancer detection," Journal of Breath Research **15**, 044002 (2021).

[3]V. Pasechnikov, S. Chukov, E. Fedorov, I. Kikuste, and M. Leja, "Gastric cancer: prevention, screening and early diagnosis," World journal of gastroenterology: WJG **20**, 13842 (2014).

[4]J. Li, Y. Peng, and Y. Duan, "Diagnosis of breast cancer based on breath analysis: An emerging method," Critical Reviews in Oncology/Hematology **87**, 28–40 (2013).

[5]M. McCulloch, T. Jezierski, M. Broffman, A. Hubbard, K. Turner, and T. Janecki, "Diagnostic accuracy of canine scent detection in early-and late-stage lung and breast cancers," Integrative cancer therapies **5**, 30–39 (2006).

[6]I. Horvath, Z. Lazar, N. Gyulai, M. Kollai, and G. Losonczy, "Exhaled biomarkers in lung cancer," European Respiratory Journal **34**, 261–275 (2009).

[7]Z. Li, J. Shu, B. Yang, Z. Zhang, J. Huang, and Y. Chen, "Emerging non-invasive detection methodologies for lung cancer," Oncology Letters **19**, 3389–3399 (2020).

[8]B. Buszewski, M. Kesy, T. Ligor, and A. Amann, "Human exhaled air analytics: biomarkers of diseases," Biomedical chromatography **21**, 553–566 (2007).

[9]R. Capuano, P. Spitalieri, R. V. Talarico, A. Catini, A. C. Domakoski, E. Martinelli, M. G. Scioli, A. Orlandi, R. Cicconi, and R. Paolesse, "Volatile compounds emission from teratogenic human pluripotent stem cells observed during their differentiation in vivo," Scientific Reports **8**, 1–12 (2018).

[10]J. S. Pyo, H. K. Ju, J. H. Park, and S. W. Kwon, "Determination of volatile biomarkers for apoptosis and necrosis by solid-phase microextraction–gas chromatography/mass spectrometry:

A pharmacometabolomic approach to cisplatin's cytotoxicity to human lung cancer cell lines," Journal of Chromatography B **876**, 170–174 (2008).

[11]A. Wehinger, A. Schmid, S. Mechtcheriakov, M. Ledochowski, C. Grabmer, G. A. Gastl, and A. Amann, "Lung cancer detection by proton transfer reaction mass-spectrometric analysis of human breath gas," International Journal of Mass Spectrometry **265**, 49–59 (2007).

[12]D. Poli, P. Carbognani, M. Corradi, M. Goldoni, O. Acampa, B. Balbi, L. Bianchi, M. Rusca, and A. Mutti, "Exhaled volatile organic compounds in patients with non-small cell lung cancer: cross sectional and nested short-term follow-up study," Respiratory Research **6**, 71 (2005).

[13]A. Ulanowska, T. Kowalkowski, E. Trawinska, and B. Buszewski, "The application of statistical methods using vocs to identify patients with lung cancer," Journal of breath research **5**, 046008 (2011).

[14]M. Ligor, T. Ligor, A. Bajtarevic, C. Ager, M. Pienz, M. Klieber, H. Denz, M. Fiegl, W. Hilbe, W. Weiss, P. Lukas, H. Jamnig, M. Hackl, B. Buszewski, W. Miekisch, J. Schubert, and A. Amann, "Determination of volatile organic compounds in exhaled breath of patients with lung cancer using solid phase microextraction and gas chromatography mass spectrometry," Clinical Chemistry and Laboratory Medicine **47**, 550–560 (2009).

[15]A. Wehinger, A. Schmid, S. Mechtcheriakov, M. Ledochowski, C. Grabmer, G. A. Gastl, and A. Amann, "Lung cancer detection by proton transfer reaction mass-spectrometric analysis of human breath gas," International Journal of Mass Spectrometry **265**, 49–59 (2007).

[16]B. Buszewski, T. Ligor, T. Jezierski, A. Wenda-Piesik, M. Walczak, and J. Rudnicka, "Identification of volatile lung cancer markers by gas chromatography–mass spectrometry: comparison with discrimination by canines," Analytical and bioanalytical chemistry **404**, 141–146 (2012).

[17]J. Ferlay, H.-R. Shin, F. Bray, D. Forman, C. Mathers, and D. M. Parkin, "Estimates of worldwide burden of cancer in 2008: Globocan 2008," International journal of cancer **127**, 2893–2917 (2010).

[18]P. Mazzone, P. Jain, A. C. Arroliga, and R. A. Matthay, "Bronchoscopy and needle biopsy techniques for diagnosis and staging of lung cancer," Clinics in Chest Medicine **23**, 137–158 (2002).

[19]G. Gregis, J.-B. Sanchez, I. Bezverkhyy, W. Guy, F. Berger, V. Fierro, J.-P. Bellat, and A. Celzard, "Detection and quantification of lung cancer biomarkers by a micro-analytical device using a single metal oxide-based gas sensor," Sensors and Actuators B: Chemical **255**, 391–400 (2018).

[20]J. Park and H. Tabata, "Gas Sensor Array Using a Hybrid Structure Based on Zeolite and Oxide Semiconductors for Multiple Bio-Gas Detection," ACS Omega **6**, 21284–21293 (2021).

[21]A. T. Güntner, S. Abegg, K. Wegner, and S. E. Pratsinis, "Zeolite membranes for highly selective formaldehyde sensors," Sensors and Actuators B: Chemical **257**, 916–923 (2018).

[22]IZA, http://www.iza-structure.org/databases/.

[23]Minerals Arranged by the New Dana Classification, http://webmineral.com/danaclass.shtml.

[24]M. Guillemot, J. Mijoin, S. Mignard, and P. Magnoux, "Volatile organic compounds (VOCs) removal over dual functional adsorbent/catalyst system," Applied Catalysis B: Environmental **75**, 249–255 (2007).

[25]Z. Zhu, H. Xu, J. Jiang, H. Wu, and P. Wu, "Hydrophobic Nanosized All-Silica Beta Zeolite: Efficient Synthesis and Adsorption Application," ACS Applied Materials & Interfaces **9**, 27273–27283 (2017).

[26]J.-P. Bellat, G. Weber, I. Bezverkhyy, and J.-F. Lamonier, "Selective adsorption of formaldehyde and water vapors in NaY and NaX zeolites," Microporous and Mesoporous Materials **288**, 109563 (2019).

[27]K. Vellingiri, J. E. Szulejko, P. Kumar, E. E. Kwon, K.-H. Kim, A. Deep, D. W. Boukhvalov, and R. J. C. Brown, "Metal organic frameworks as sorption media for volatile and semi-volatile organic compounds at ambient conditions," Scientific Reports **6**, 27813 (2016).

[28]G. da Silva, J. Simon, and J. M. Salazar, "When less is more: does more na+-cations mean more adsorption sites for toluene in faujasites?" Physical Chemistry Chemical Physics **25**, 8028–8042 (2023).

[29]M. Shamzhy, M. Opanasenko, P. Concepcin, and A. Martnez, "New trends in tailoring active sites in zeolite-based catalysts," Chem. Soc. Rev. **48**, 1095–1149 (2019).

[30]R. Krishna and J. M. van Basten, "Water/Alcohol Mixture Adsorption in Hydrophobic Materials: Enhanced Water Ingress Caused by Hydrogen Bonding | ACS Omega," ACS Omega **5**, 28393–28402 (2020).

[31]Y. Zhi, H. Shi, L. Mu, Y. Liu, D. Mei, D. M. Camaioni, and J. A. Lercher, "Dehydration Pathways of 1-Propanol on HZSM-5 in the Presence and Absence of Water," Journal of the American Chemical Society **137**, 15781–15794 (2015).

[32]K. Sato, K. Aoki, K. Sugimoto, K. Izumi, S. Inoue, J. Saito, S. Ikeda, and T. Nakane, "Dehydrating performance of commercial LTA zeolite membranes and application to fuel grade bioethanol production by hybrid distillation/vapor permeation process," Microporous and Mesoporous Materials 4th International Zeolite Membrane Meeting, **115**, 184–188 (2008).

[33]K. Sato, K. Sugimoto, N. Shimotsuma, T. Kikuchi, T. Kyotani, and T. Kurata, "Development of practically available up-scaled high-silica CHA-type zeolite membranes for industrial purpose in dehydration of N-methyl pyrrolidone solution," Journal of Membrane Science **409-410**, 82–95 (2012).

[34]R. Li, S. Chong, N. Altaf, Y. Gao, B. Louis, and Q. Wang, "Synthesis of ZSM-5/Siliceous Zeolite Composites for Improvement of Hydrophobic Adsorption of Volatile Organic Compounds," Frontiers in Chemistry **7**, 505 (2019).

[35]A. F. Cosseron, T. J. Daou, L. Tzanis, H. Nouali, I. Deroche, B. Coasne, and V. Tchamber, "Adsorption of volatile organic compounds in pure silica CHA, BEA, MFI and STT-type zeolites," Microporous and Mesoporous Materials **173**, 147–154 (2013).

[36]M. Guillemot, J. Mijoin, S. Mignard, and P. Magnoux, "Adsorption of tetrachloroethylene (PCE) in gas phase on zeolites of faujasite type: Influence of water vapour and of Si/Al ratio," Microporous and Mesoporous Materials **111**, 334–342 (2008).

[37]O. Schäf, V. Wernert, H. Ghobarkar, and P. Knauth, "Microporous Stilbite single crystals for alcohol sensing," Journal of Electroceramics **16**, 93–98 (2006).

[38]A. J. Schwanke, R. Balzer, and S. Pergher, "Degradation of volatile organic compounds with catalysts-containing zeolite and ordered mesoporous silica," in *Handbook of Ecomaterials*, edited by L. M. T. Martínez, O. V. Kharissova, and B. I. Kharisov (Springer International Publishing, Cham, 2017) pp. 1–12.

[39]P. Gómez-Álvarez, E. G. Noya, E. Lomba, S. Valencia, and J. Pires, "Study of Short-Chain Alcohol and AlcoholWater Adsorption in MEL and MFI Zeolites," Langmuir **34**, 12739–12750 (2018).

[40]R. Krishna and J. M. van Baten, "Entropy-based separation of linear chain molecules by exploiting differences in the saturation capacities in cage-type zeolites," Separation and purification technology **76**, 325–330 (2011).

[41]R. Krishna and J. M. van Baten, "Hydrogen bonding effects in adsorption of water- alcohol mixtures in zeolites and the consequences for the characteristics of the maxwell- stefan diffusivities," Langmuir **26**, 10854–10867 (2010).

[42]M. Sakuth, J. Meyer, and J. Gmehling, "Vapor Phase Adsorption Equilibria of Toluene + 1-Propanol Mixtures on Y-Zeolites with Different Silicon to Aluminum Ratios," Journal of Chemical & Engineering Data **40**, 895–899 (1995).

[43]J.-P. Bellat, G. Weber, I. Bezverkhyy, and J.-F. Lamonier, "Selective adsorption of formaldehyde and water vapors in nay and nax zeolites," Microporous and Mesoporous Materials **288**, 109563 (2019).

[44]G. Weber, I. Bezverkhyy, J.-P. Bellat, A. Ballandras, G. Or-

tiz, G. Chaplais, J. Patarin, F.-X. Coudert, A. H. Fuchs, and A. Boutin, "Mechanism of water adsorption in the large pore form of the gallium-based mil-53 metal-organic framework," Microporous and Mesoporous Materials **222**, 145–152 (2016).

[45]F.-X. Coudert, A. U. Ortiz, V. Haigis, D. Bousquet, A. H. Fuchs, A. Ballandras, G. Weber, I. Bezverkhyy, N. Geoffroy, and J.-P. Bellat, "Water adsorption in flexible gallium-based mil-53 metal-organic framework," The Journal of Physical Chemistry C **118**, 5397–5405 (2014).

[46]M.-H. Simonot-Grange, A. Elm'Chaouri, G. Weber, P. Dufresne, F. Raatz, and J.-F. Joly, "Characterization of the dealumination effect into h faujasites by adsorption: Part 1. the water molecule as a structural aluminum ion selective probe," Zeolites **12**, 155–159 (1992).

[47]J. McBain and A. Bakr, "A new sorption balance1," Journal of the American Chemical Society **48**, 690–695 (1926).

[48]G. Weber, E. Sciora, J. Guichard, F. Bouyer, I. Bezverkhyy, F. Bernard, H. Lecoq, R. Besnard, and J.-P. Bellat, "New insight on the lithium hydride–water vapor reaction system," international journal of hydrogen energy **43**, 22557–22567 (2018).

[49]Y. Nejahi, M. Soroush Barhaghi, J. Mick, B. Jackman, K. Rushaidat, Y. Li, L. Schwiebert, and J. Potoff, "Gomc: Gpu optimized monte carlo for the simulation of phase equilibria and physical properties of complex fluids," SoftwareX **9**, 20–27 (2019).

[50]P. Bai, M. Tsapatsis, and J. I. Siepmann, "Trappe-zeo: Transferable potentials for phase equilibria force field for all-silica zeolites," The Journal of Physical Chemistry C **117**, 24375–24387 (2013).

[51]B. Chen, J. J. Potoff, and J. I. Siepmann, "Monte carlo calculations for alcohols and their mixtures with alkanes. transferable potentials for phase equilibria. 5. united-atom description of primary, secondary, and tertiary alcohols," The Journal of Physical Chemistry B **105**, 3093–3104 (2001).

[52]J. G. Harris and K. H. Yung, "Carbon dioxide's liquid-vapor coexistence curve and critical properties as predicted by a simple molecular model," The Journal of Physical Chemistry **99**, 12021–12024 (1995).

[53]C. Murthy, K. Singer, M. Klein, and I. McDonald, "Pairwise additive effective potentials for nitrogen," Molecular Physics **41**, 1387–1399 (1980).

[54]J. L. Abascal and C. Vega, "A general purpose model for the condensed phases of water: Tip4p/2005," The Journal of chemical physics **123**, 234505 (2005).

[55]J. M. Castillo, J. Silvestre-Albero, F. Rodriguez-Reinoso, T. J. Vlugt, and S. Calero, "Water adsorption in hydrophilic zeolites: experiment and simulation," Physical Chemistry Chemical Physics **15**, 17374–17382 (2013).

[56]A. Di Lella, N. Desbiens, A. Boutin, I. Demachy, P. Ungerer, J.-P. Bellat, and A. H. Fuchs, "Molecular simulation studies of water physisorption in zeolites," Physical Chemistry Chemical Physics **8**, 5396–5406 (2006).

[57]J. Perez-Carbajo, S. R. Balestra, S. Calero, and P. J. Merkling, "Effect of lattice shrinking on the migration of water within zeolite lta," Microporous and Mesoporous Materials **293**, 109808 (2020).

[58]A. Al Ezzi and H. Ma, "Equilibrium adsorption isotherm mechanism of water vapor on zeolites 3a, 4a, x, and y," in *ASME International Mechanical Engineering Congress and Exposition*, Vol. 58417 (American Society of Mechanical Engineers, 2017) p. V006T08A059.

[59]T. Ammouli, J.-L. Paillaud, H. Nouali, R. Stephan, M.-C. Hanf, P. Sonnet, and I. Deroche, "Insights into water adsorption in potassium-exchanged x-type faujasite zeolite: molecular simulation and experiment," The Journal of Physical Chemistry C **125**, 19405–19416 (2021).

[60]M. J. Purdue and Z. Qiao, "Molecular simulation study of wet flue gas adsorption on zeolite 13x," Microporous and Mesoporous Materials **261**, 181–197 (2018).

[61]"SAT-TMMC: Liquid-Vapor coexistence properties - TIP4P/2005 Water (LRC)," NIST, https://www.nist.gov/mml/csd/chemical-informatics-group/sat-tmmc-liquid-vapor-coexistence-properties-tip4p2005-water-lrc (2016).

[62]T. Zhou, P. Bai, J. I. Siepmann, and A. E. Clark, "Deconstructing the confinement effect upon the organization and dynamics of water in hydrophobic nanoporous materials: Lessons learned from zeolites," The Journal of Physical Chemistry C **121**, 22015–22024 (2017).

[63]M. Trzpit, M. Soulard, J. Patarin, N. Desbiens, F. Cailliez, A. Boutin, I. Demachy, and A. Fuchs, "The effect of local defects on water adsorption in silicalite-1 zeolite: A joint experimental and molecular simulation study," Langmuir **23**, 10131–10139 (2007).

[64]F. Cailliez, G. Stirnemann, A. Boutin, I. Demachy, and A. H. Fuchs, "Does water condense in hydrophobic cavities? a molecular simulation study of hydration in heterogeneous nanopores," The Journal of Physical Chemistry C **112**, 10435–10445 (2008).

[65]K.-M. Kim, H.-T. Oh, S.-J. Lim, K. Ho, Y. Park, and C.-H. Lee, "Adsorption equilibria of water vapor on zeolite 3a, zeolite 13x, and dealuminated y zeolite," Journal of Chemical & Engineering Data **61**, 1547–1554 (2016).

[66]P. Moura, E. Rodríguez-Aguado, D. Maia, D. Melo, R. Singh, S. Valencia, P. Webley, F. Rey, M. Bastos-Neto, and E. Rodríguez-Castellón, "Water adsorption and hydrothermal stability of cha zeolites with different si/al ratios and compensating cations," Catalysis Today **390**, 99–108 (2022).

[67]K.-M. Kim, H.-T. Oh, S.-J. Lim, K. Ho, Y. Park, and C.-H. Lee, "Adsorption Equilibria of Water Vapor on Zeolite 3A, Zeolite 13X, and Dealuminated Y Zeolite," Journal of Chemical & Engineering Data **61**, 1547–1554 (2016).

[68]M. Fleys, R. W. Thompson, and J. C. MacDonald, "Comparison of the behavior of water in silicalite and dealuminated zeolite y at different temperatures by molecular dynamic simulations," The Journal of Physical Chemistry B **108**, 12197–12203 (2004).

[69]T. D. Pham, R. Xiong, S. I. Sandler, and R. F. Lobo, "Experimental and computational studies on the adsorption of CO2 and N2 on pure silica zeolites," Microporous and Mesoporous Materials **185**, 157–166 (2014).

[70]H. Fang, P. Kamakoti, J. Zang, S. Cundy, C. Paur, P. I. Ravikovitch, and D. S. Sholl, "Prediction of CO_2 adsorption properties in zeolites using force fields derived from periodic dispersion-corrected DFT calculations," The Journal of Physical Chemistry C **116**, 10692–10701 (2012).

[71]G. Maurin, P. Llewellyn, and R. Bell, "Adsorption mechanism of carbon dioxide in faujasites: grand canonical monte carlo simulations and microcalorimetry measurements," The Journal of Physical Chemistry B **109**, 16084–16091 (2005).

[72]H. Thamm, "Calorimetric study on the state of c1–c4 alcohols sorbed on silicalite," Journal of the Chemical Society, Faraday Transactions 1: Physical Chemistry in Condensed Phases **85**, 1 (1989).

[73]A. Giaya and R. W. Thompson, "Single-component gas phase adsorption and desorption studies using a tapered element oscillating microbalance," Microporous and Mesoporous Materials **55**, 265–274 (2002).

[74]T. Golden and S. Sircar, "Gas Adsorption on Silicalite," Journal of Colloid and Interface Science **162**, 182–188 (1994).

[75]R. Xiong, S. I. Sandler, and D. G. Vlachos, "Molecular screening of alcohol and polyol adsorption onto mfi-type zeolites," Langmuir **28**, 4491–4499 (2012).

[76]P. Demontis, G. Stara, and G. B. Suffritti, "Behavior of Water in the Hydrophobic Zeolite Silicalite at Different Temperatures. A Molecular Dynamics Study," The Journal of Physical Chemistry B **107**, 4426–4436 (2003).

[77]J. Puibasset and R. J.-M. Pellenq, "Grand Canonical Monte Carlo Simulation Study of Water Adsorption in Silicalite at 300 K," The Journal of Physical Chemistry B **112**, 6390–6397 (2008).

[78]I. Wadsö, "Heats of vaporization for a number of organic compounds at 25 c," Acta Chem. Scand **20**, 544 (1966).

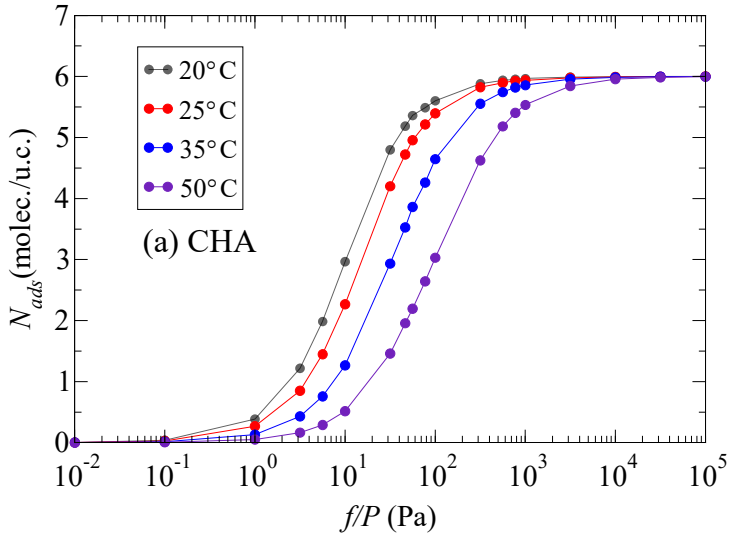

(a) Chabazite

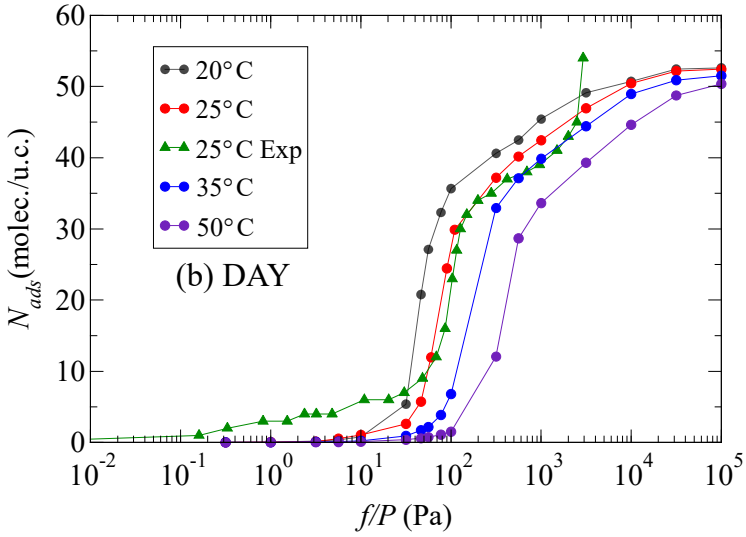

(b) DAY

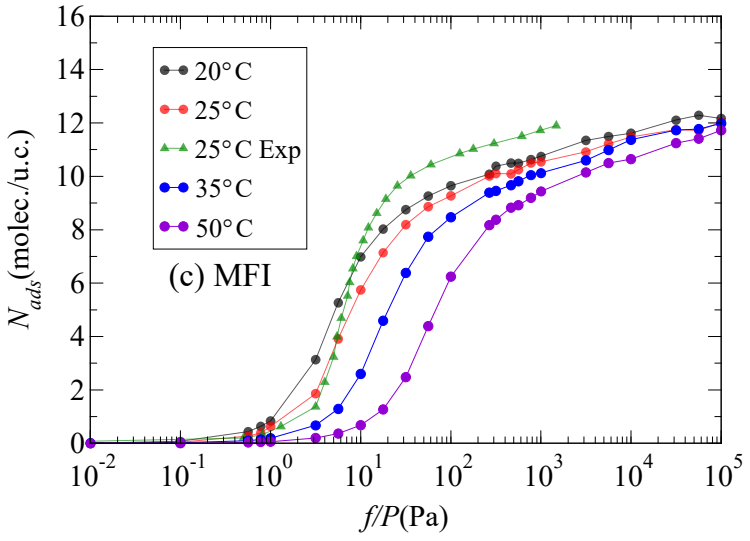

(c) Silicalite-1

FIG. 2: Adsorption isotherms of C_3H_8O on three different zeolites chabazite (a), DAY (b), silicalite-1 (c) at 20, 25, 35 and 50°C (the abscisse scale refers to fugacity for simulated data and to pressure for experimental data).

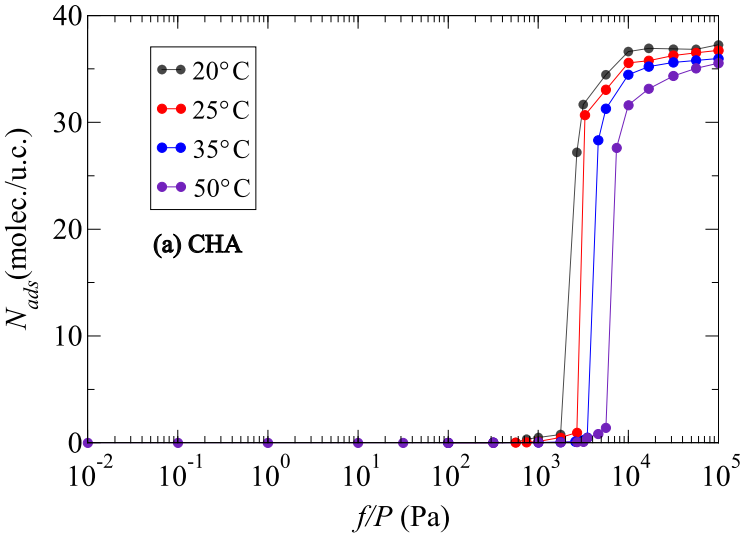

(a) Chabazite

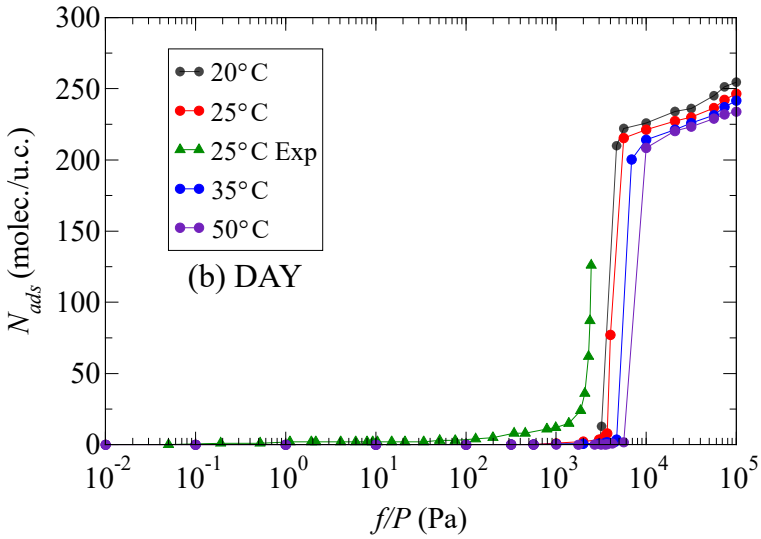

(b) DAY

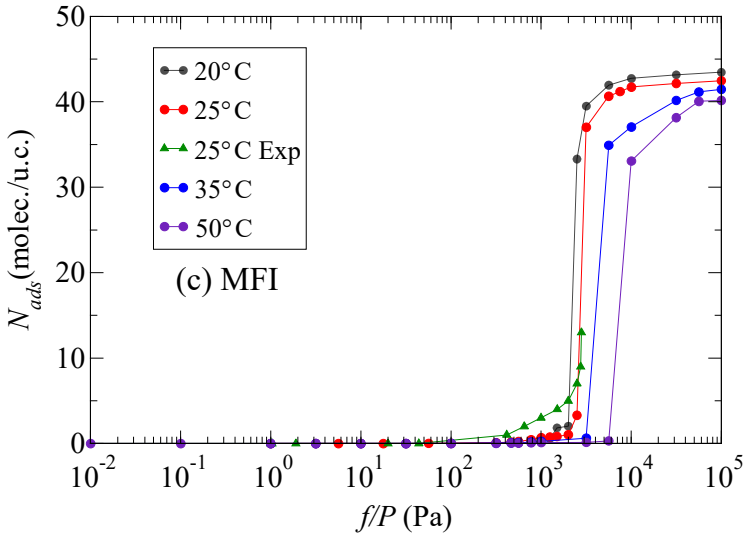

FIG. 3: Same legend as Fig. 2 for H_2O.

(c) Silicalite-1

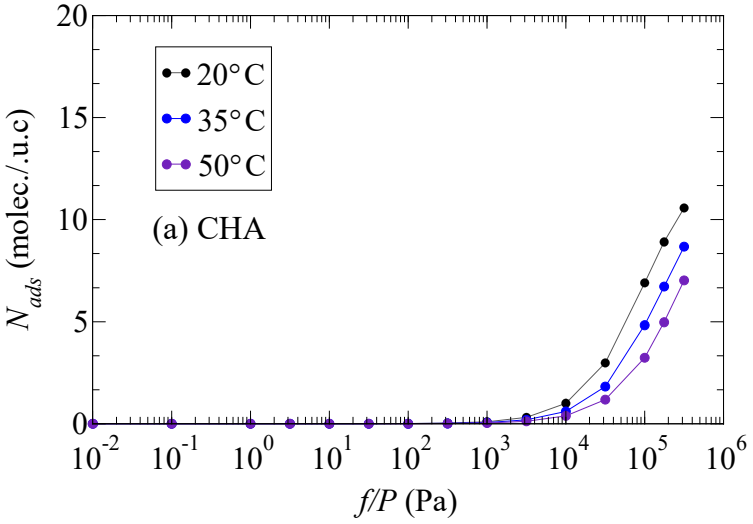

(a) Chabazite

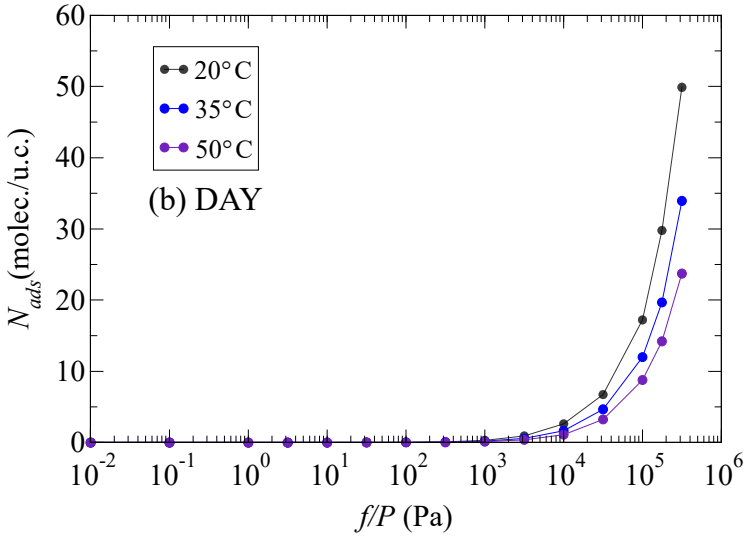

(b) DAY

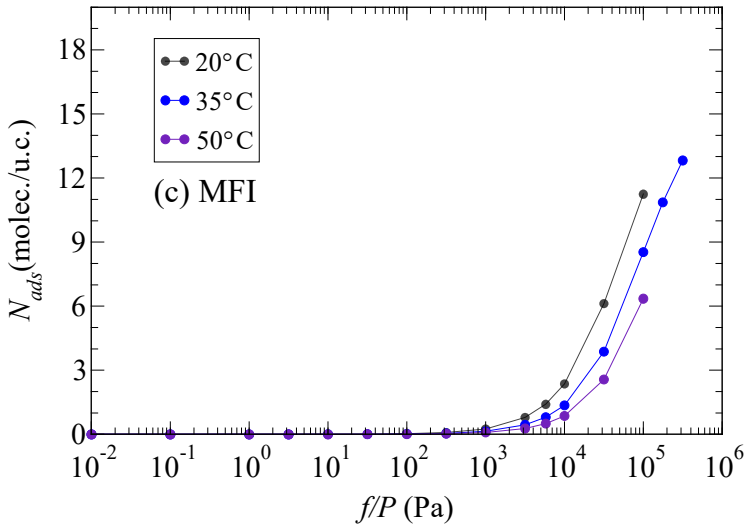

(c) Silicalite-1

FIG. 4: Same legend as Fig. 2 for carbon dioxide (without results at 25°C).

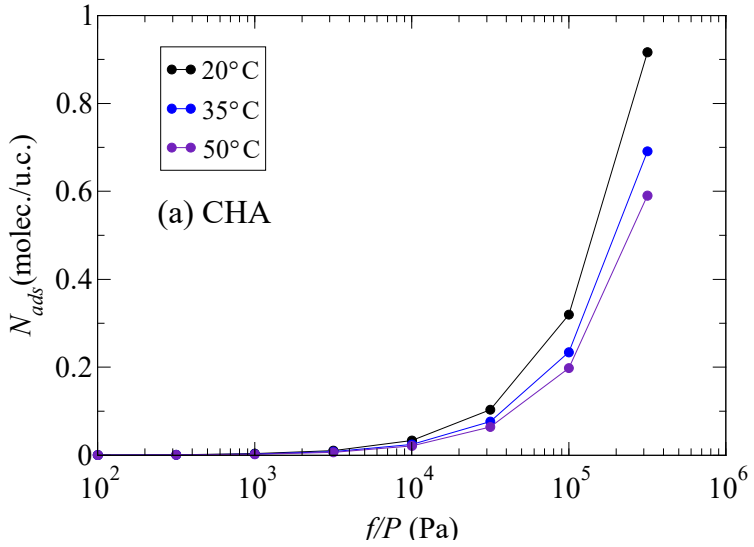

(a) Chabazite

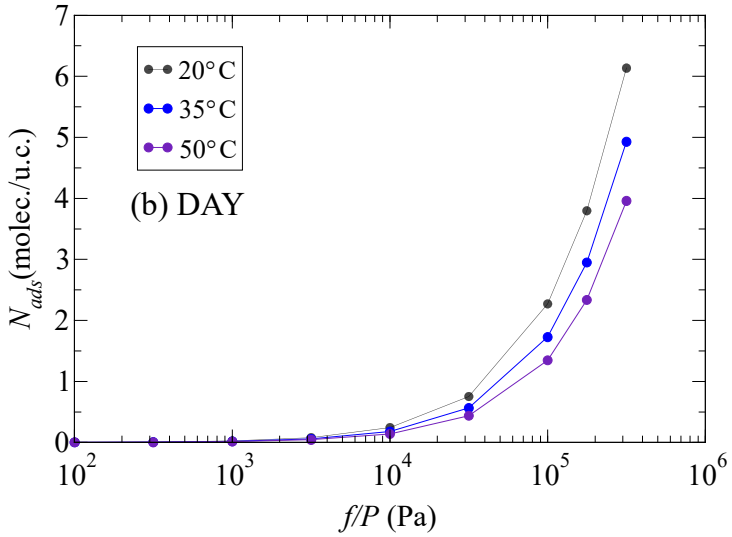

(b) DAY

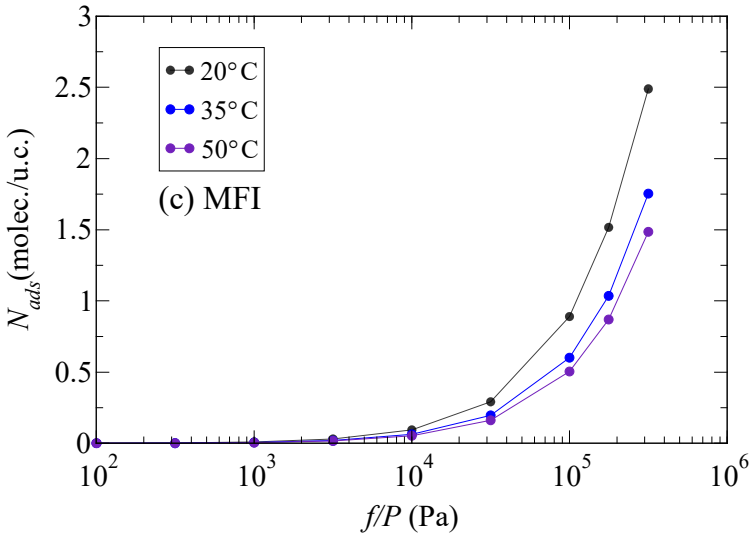

(c) Silicalite-1

FIG. 5: Same legend as Fig. 2 for nitrogen (without results at 25°C).

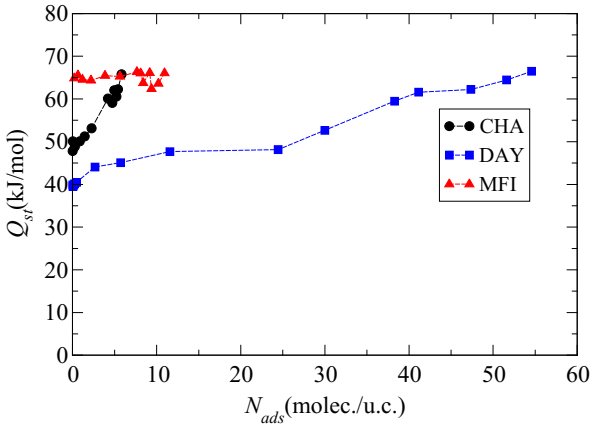

(a) Propanol

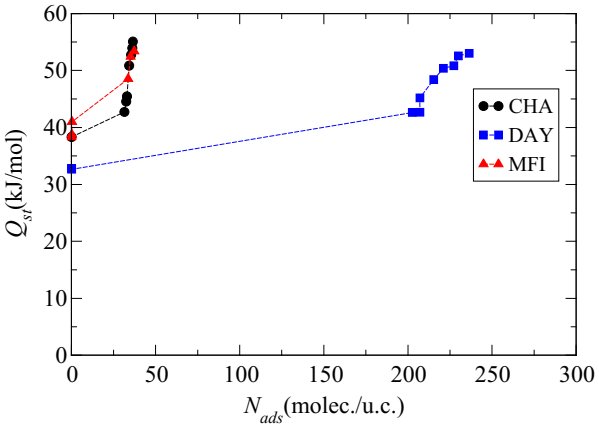

(b) Water

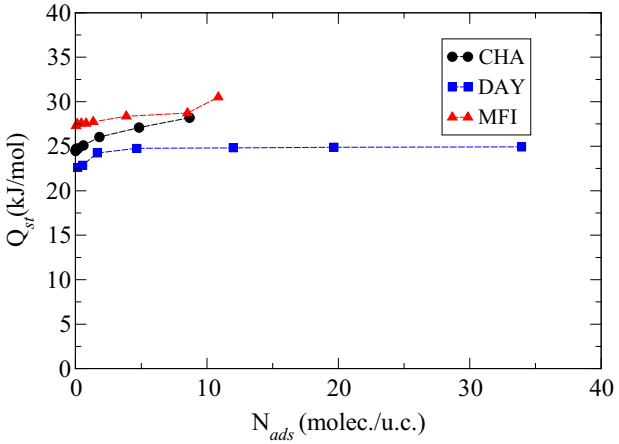

(c) Carbon dioxide

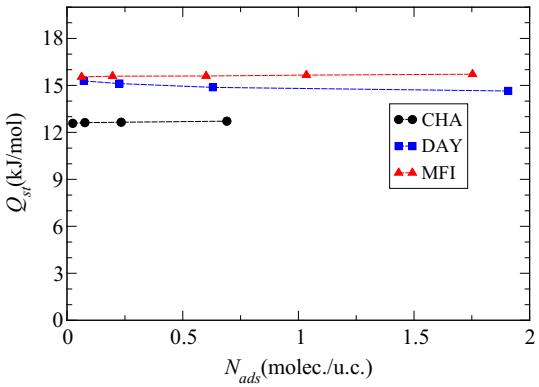

(d) Nitrogen

FIG. 6: 1-Propanol (a), water (b), carbon dioxide (c) and nitrogen (d) heat of adsorption as function of loading, on the three investigated zeolite structures (CHA:circle, DAY:square, MFI:triangle up).

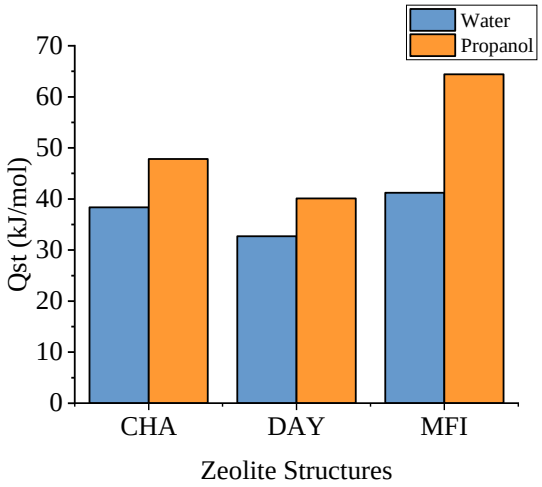

FIG. 7: Comparison of the 1-propanol and water heats of adsorption at zero loading, on the three investigated zeolite structures.

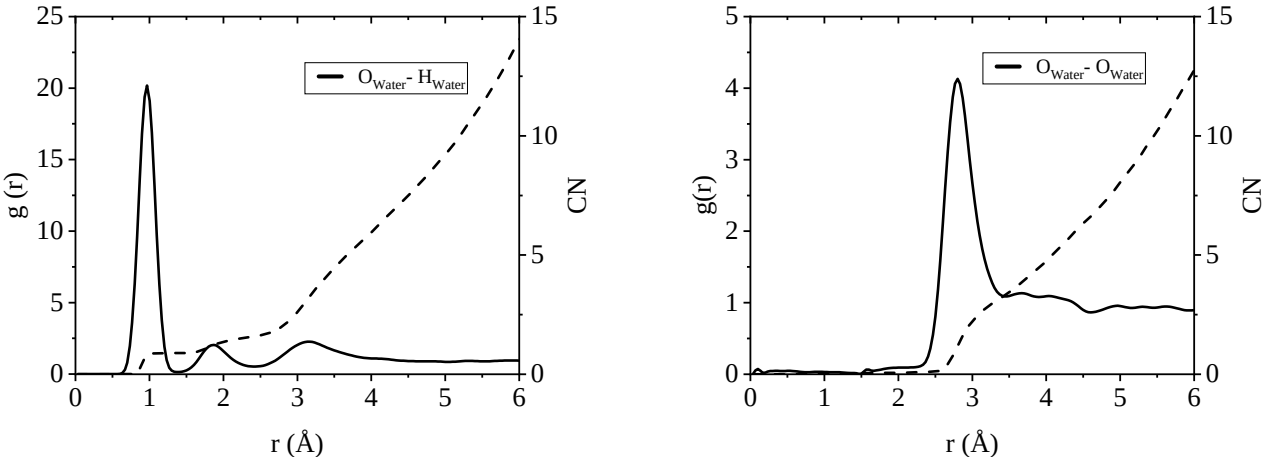

(a) OH (b) OO

FIG. 8: Radial distribution function (full line) and the running coordination number (dashed line) of water on chabazite at saturation (at 10^5Pa), (a) rdf between Hydrogen and the Oxygen of the Water, (b) rdf between Oxygen of Water molecule.

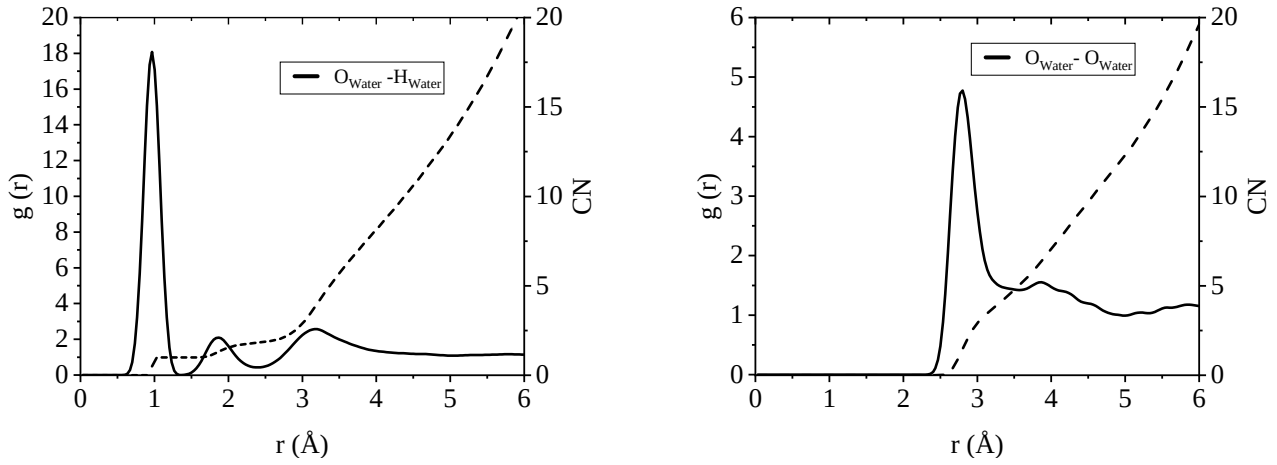

(a) OH (b) OO

FIG. 9: Radial distribution function (full line) and the running coordination number (dashed line) of water on DAY at saturation (at 10^5Pa), (a) rdf between Hydrogen and the Oxygen of the Water, (b) rdf between Oxygen of Water molecule.

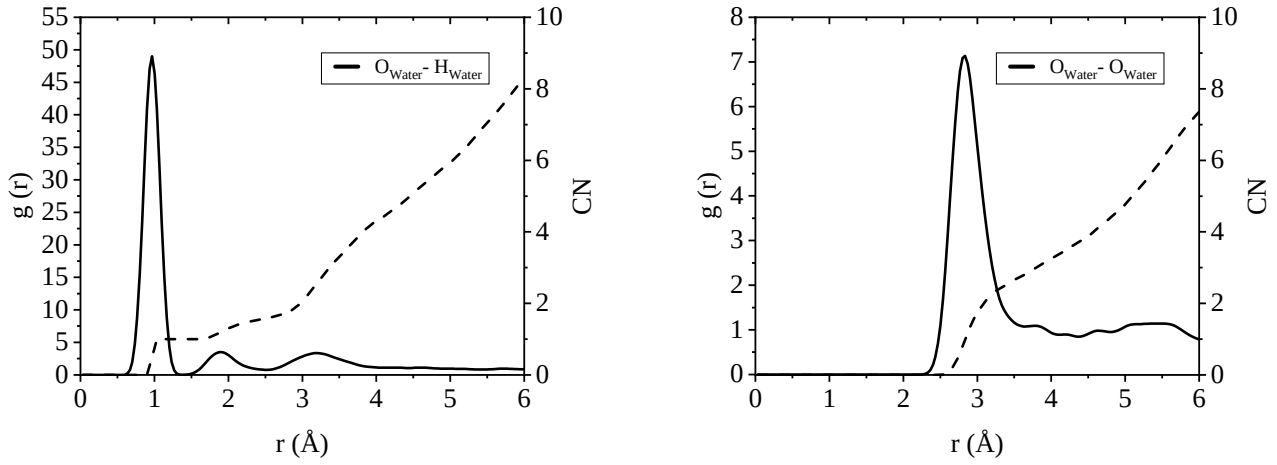

(a) OH (b) OO

FIG. 10: Radial distribution function (full line) and the running coordination number (dashed line) of water on MFI at saturation (at 10^5Pa), (a) rdf between Hydrogen and the Oxygen of the Water, (b) rdf between Oxygen of Water molecule.

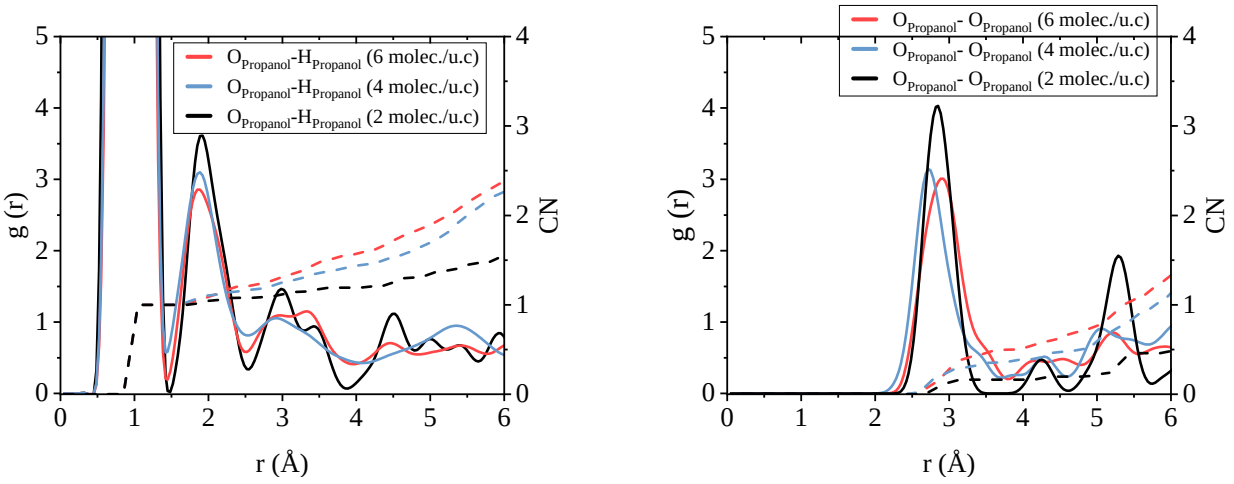

(a) OH (b) OO

FIG. 11: Radial distribution function (full line) and the running coordination number (dashed line) of 1-propanol on CHA at different loading, (a) rdf between the Hydrogen and the Oxygen of the Propanol, (b) rdf between Oxygen of the Propanol.

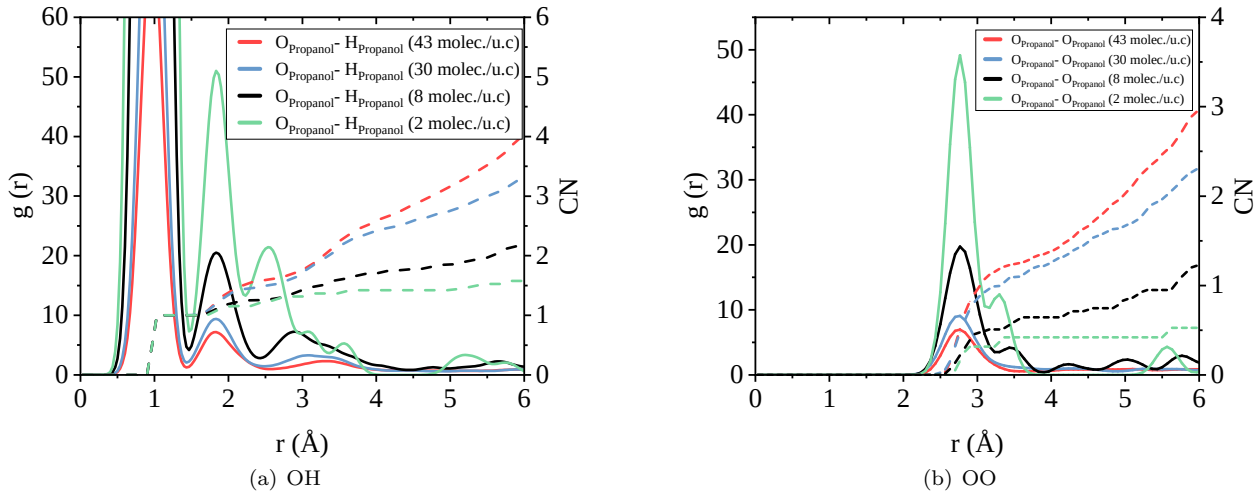

(a) OH (b) OO

FIG. 12: Radial distribution function (full line) and the running coordination number (dashed line) of 1-propanol on DAY at different loading, (a) rdf between the Hydrogen and the Oxygen of the Propanol, (b) rdf between Oxygen of the Propanol.

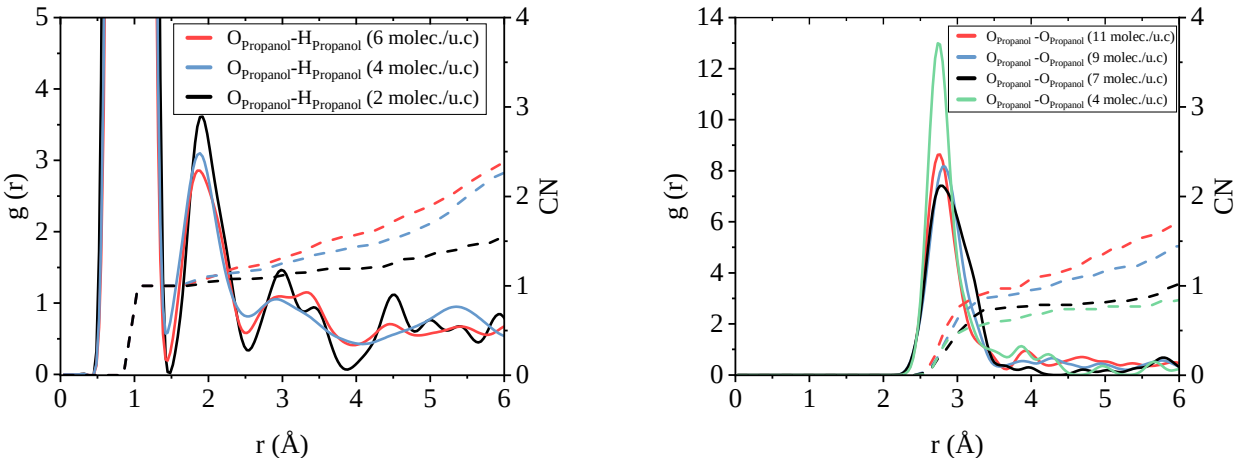

(a) OH (b) OO

FIG. 13: Radial distribution function (full line) and the running coordination number (dashed line) of 1-propanol on MFI at different loading, (a) rdf between the Hydrogen and the Oxygen of the Propanol, (b) rdf between Oxygen of the Propanol.